The Astrophysical Journal Letters, 889:L11 (6pp), 2020 January 20 https://doi.org/10.3847/2041-8213/ab63de

First Detection of the [O I] 63 μm Emission from a Redshift 6 Dusty Galaxy

Matus Rybak[1], J. A. Zavala[2], J. A. Hodge[1], C. M. Casey[2], and P. van der Werf[1]
[1] Leiden Observatory, Leiden University, Niels Bohrweg 2, 2333 CA Leiden, The Netherlands; mrybak@strw.leidenuniv.nl
[2] Department of Astronomy, The University of Texas at Austin, 2515 Speedway Boulevard Stop C1400, Austin, TX 78712, USA
Received 2019 November 11; revised 2019 December 10; accepted 2019 December 19; published 2020 January 20

Abstract

We report a ground-based detection of the [O I] 63 μm line in a $z = 6.027$ gravitationally lensed dusty star-forming galaxy (DSFG) G09.83808 using the Atacama Pathfinder EXperiment SEPIA 660 receiver, the first unambiguous detection of the $[O\,I]_{63}$ line beyond redshift 3, and the first obtained from the ground. The $[O\,I]_{63}$ line is robustly detected at 22 ± 5 Jy km s^{-1}, corresponding to an intrinsic (de-lensed) luminosity of $(5.4 \pm 1.3) \times 10^9\,L_\odot$. With the $[O\,I]_{63}$/[C II] luminosity ratio of 4, the $[O\,I]_{63}$ line is the main coolant of the neutral gas in this galaxy, in agreement with model predictions. The high $[O\,I]_{63}$ luminosity compensates for the pronounced [C II] deficit ($[C\,II]/FIR \simeq 4 \times 10^{-4}$). Using photon-dominated region models, we derive a source-averaged gas density $n = 10^{4.0}$ cm^{-3}, and FUV field strength $G = 10^4\,G_0$, comparable to the $z = 2$–4 DSFG population. If G09.83808 represents a typical high-redshift DSFG, the $[O\,I]_{63}$ line from $z = 6$ non-lensed DSFGs should be routinely detectable in the Atacama Large Millimeter/submillimeter Array Band 9 observations with ~15 minutes on-source, opening a new window to study the properties of the earliest DSFGs.

Unified Astronomy Thesaurus concepts: Submillimeter astronomy (1647); High-redshift galaxies (734); Ultraluminous infrared galaxies (1735)

1. Introduction

Although thousands of the submillimeter bright, dusty star-forming galaxies (DSFGs) have been discovered at $z = 2$–5 (e.g., Casey et al. 2014), the number of known DSFGs drops precipitously at $z \geqslant 5$: only a handful of $z \geqslant 6$ DSFGs have been discovered to date (Riechers et al. 2013; Decarli et al. 2017; Strandet et al. 2017; Zavala et al. 2018b). These dust-laden sources provide evidence for intense star formation and interstellar medium (ISM) enrichment within the first Gyr of cosmic history, and extremely efficient baryon conversion. Characterizing the conditions of their star-forming ISM—particularly the gas density of the star-forming clouds and the FUV radiation field illuminating them—is a key to understanding these extreme sources.

Far-IR fine-structure lines of [C II], [O I], and [C I] and the CO rotational lines are the key diagnostics of the neutral and molecular gas in the star-forming clouds. By comparing the observed line and continuum fluxes to photochemical models, the ISM properties such as the gas density (n) and the strength of the incident FUV radiation (G) can be inferred. Indeed, CO and [C II] lines have been instrumental in studying the ISM of $z = 2$–5 DSFGs (e.g., Stacey et al. 2010; Gullberg et al. 2015; Wardlow et al. 2017; Zhang et al. 2018; Rybak et al. 2019a) down to sub-kiloparsec scales (Lamarche et al. 2018; Rybak et al. 2019b; Yang et al. 2019); these have revealed a dense ISM (n=10^3–10^5 cm^{-3}) exposed to strong FUV fields ($G = 10^2$–$10^5\,G_0$).[3]

At $z \geqslant 5$, our toolkit for studying the neutral star-forming ISM becomes much more limited. While the Atacama Large Millimeter/submillimeter Array (ALMA) has enabled routine studies of the [C II] 158 μm (e.g., Decarli et al. 2017; Smit et al. 2018) and [O III] 88 μm emission (e.g., Inoue et al. 2016; Carniani et al. 2017; Hashimoto et al. 2019; Harikane et al. 2019), the former arises from both the ionized and neutral ISM, while the latter is associated with H II regions. The low-J CO lines become extremely difficult to detect due to both their intrinsic faintness and the elevated cosmic microwave background (CMB) temperature (e.g., da Cunha et al. 2013). Although mid-J CO lines remain detectable at $z \geqslant 5$, their interpretation is sensitive to the details of radiative transfer assumptions (e.g., optical depth and turbulence; Popping et al. 2019) and the CMB background (da Cunha et al. 2013).

However, in a dense, warm ISM—such as that in DSFGs or present-day (ultra)luminous infrared galaxies (ULIRGs)—the [O I] 63 μm line ($[O\,I]_{63}$) overtakes [C II] as the main gas cooling channel (Kaufman et al. 1999, 2006; Narayanan & Krumholz 2017). With a critical density $n_{crit} \simeq 5 \times 10^5$ cm^{-3}, $[O\,I]_{63}$ traces much denser ISM than the [C II] emission ($n_{crit} = 3 \times 10^3$ cm^{-3} for collisions with hydrogen in PDRs). Indeed, cosmological hydrodynamical simulations (e.g., Olsen et al. 2017; Katz et al. 2019) predict $[O\,I]_{63}$ to be the most luminous FIR line in star-forming galaxies at the highest redshifts. Unlike CO emission, the $[O\,I]_{63}$ line is not strongly affected by the CMB background and local excitation conditions; and unlike [C II], it is directly associated with the neutral ISM.

Ground-based studies of the $[O\,I]_{63}$ emission at $z \geqslant 1$ have been limited by the atmospheric absorption at submillimeter wavelengths. Above the atmosphere, the $[O\,I]_{63}$ emission from $z \sim 0$ ULIRGs has been extensively studied with *Infrared Space Observatory* (Brauher et al. 2008) and *Herschel* (Graciá-Carpio et al. 2011; Díaz-Santos et al. 2017; Herrera-Camus et al. 2018a). Unfortunately, at $z \geqslant 1$, the limited collecting area and on-source time resulted in only ~15 $[O\,I]_{63}$ detections (Ivison et al. 2010; Sturm et al. 2010; Coppin et al. 2012; Brisbin et al. 2015; Wardlow et al. 2017; Zhang et al. 2018), mainly in gravitationally lensed galaxies, and only out to $z \simeq 3$ (Zhang et al. 2018). However, at $z \geqslant 5.5$, $[O\,I]_{63}$ is redshifted into ALMA Band 10, and at $z \geqslant 6.0$, into ALMA/Atacama Pathfinder EXperiment (APEX) Band 9, making it observable from the ground. In this Letter, we report the first ground-based

[3] The far-UV field strength is given in Habing field units, $1\,G_0 = 1.6 \times 10^{-3}$ erg s^{-1} cm^{-2}, a typical value for the Galactic interstellar FUV field.

detection of the [O I]$_{63}$ line from a $z = 6.027$ strongly lensed DSFG, achieved using APEX SEPIA 660 spectroscopy.

2. Observations

We targeted G09.83808 (J2000 09:00:45.8+00:41:23), a $z = 6.027$ strongly gravitationally lensed DSFG,[4] discovered in the *Herschel* H-ATLAS survey. Zavala et al. (2018b) obtained a robust spectroscopic confirmation from [C II] (Submillimeter Array (SMA)) and CO (5–4)/(6–5) and H_2O lines (Large Millimeter Telescope). Using high-resolution ALMA Band 7 imaging, Zavala et al. (2018b) confirmed that G09.83808 is strongly gravitationally lensed, with an FIR magnification $\mu_{\rm FIR} \simeq 9$. Based on the FIR and millimeter-wave spectroscopy, G09.83808 has a source-plane FIR luminosity $L_{\rm FIR} = (3.8 \pm 0.5) \times 10^{12}\ L_\odot$ (8–1000 μm), corresponding to a star formation rate (SFR) of $\sim$650 $M_\odot$ yr^{-1} (assuming the Salpeter initial mass function (IMF); Kennicutt 1998). Due to its strongly lensed nature and fortuitous redshift, G09.83808 is ideally suited for [O I]$_{63}$ observations.

The observations were carried out using the APEX 12 m telescope, and the Swedish ESO PI (SEPIA) Band 9 receiver (Belitsky et al. 2018; Hesper et al. 2017, 2018), as a part of the NOVA Guaranteed Time Observations (Proposal 0104.B-0551, PI: Rybak).

The observations were carried out in two blocks: 2019 October 28 (5.6 hr total time, 97 minutes on-source, source elevation 41°–66°) and 2019 November 6 (2.6 hr total time, 36 minutes on-source, source elevation 39°–70°).

The observations were conducted in an on/off mode, with the secondary wobbler frequency of 1.5 Hz. For the 2019 October 28 observations, the initial pointing and calibration was done on R Dor; for the 2019 November 6 observations, using o-Ceti. The bandpass calibration and intermediate calibration and pointing checks were performed using IRC +10216 on both dates. Two scans on 2019 October 28 were aborted due to tracking errors.

The observing conditions were excellent, with the precipitable water vapor of 0.45–0.55 mm (2019 October 28) and 0.30–0.35 mm (2019 November 6), corresponding to an atmospheric transmission of 0.6–0.8 at 675.2 GHz. The total observing time was 8.2 hr, with 133 minutes on-source time.

The frequency setup consisted of two sidebands, each consisting of two spectrometers with 4096 channels 0.9765 MHz (0.43 km s^{-1}) wide, giving a total bandwidth of 8 GHz per sideband. For both the 2019 October 28 and November 6 observations, we used two separate tunings with the line-containing spectrometer centered at 673.920 GHz (44.3 minutes on-source) and 674.920 GHz GHz (53.1 minutes on-source), respectively.

At the observed line frequency of 675.220 GHz, the APEX primary beam FWHM is 9.″2, compared to the G09.83808 image separation of $\sim$2″. Although DSFGs show high multiplicity (e.g., Hodge et al. 2013; Decarli et al. 2017), the high-resolution SMA ($\sim$2″) and ALMA imaging ($\sim$1.″2) did not detect an FIR- or [C II]-bright companion source to G09.83808. The observed [O I]$_{63}$ emission can be thus unambiguously assigned to G09.83808.

[4] Adopting a flat ΛCDM cosmology from Planck Collaboration et al. (2016), $z = 6.027$ corresponds to a luminosity distance of 59350 Mpc and the age of universe of 0.94 Gyr (Wright 2006).

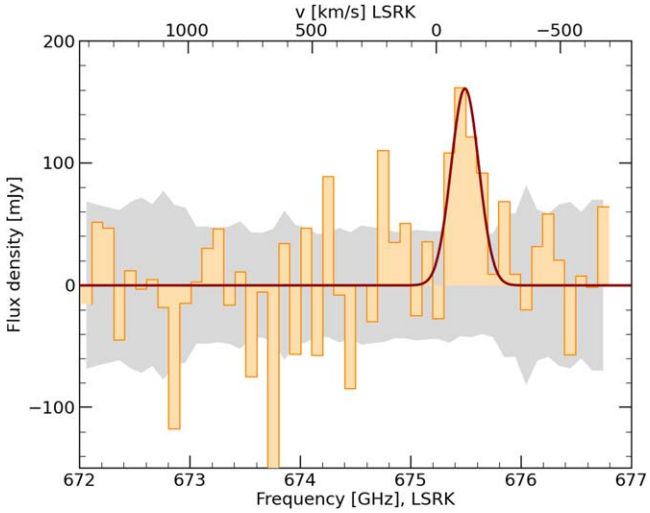

Figure 1. APEX SEPIA 660 spectrum of G09.83808, resampled into 100 MHz (45 km s^{-1}) bins. The best-fitting Gaussian profile is indicated in red; the gray shading indicates the rms noise. The line is detected at $\sim 4\sigma$ level over 100 MHz channels, and $\sim 5\sigma$ over 225 MHz (100 km s^{-1}) channels.

The data were reduced using the GILDAS CLASS package.[5] Each tuning was processed separately, before combining the data. The two linear polarizations were combined into the Stokes *I*. After windowing the channels containing the line or the atmospheric lines, we subtract the continuum by fitting a linear slope to the central 98% channels of each integration, before combining the data together.

3. Results and Discussion

3.1. Line Detection

We detect the [O I]$_{63}$ line at 675.45 GHz[6] (Figure 1), with a peak flux of 2.3 ± 0.6 mK for 44 km s^{-1} binning (100 MHz, 3.9σ detection) and 2.08 ± 0.40 mK (5.3σ) for 100 km s^{-1} (225 MHz) binning. The line is separately detected at 3.8σ (100 MHz bandwidth) in the 2019 October 28 scan. The signal is well separated from the O_3 atmospheric lines at 673.9, 676.1, and 679.3 GHz. We derive the [O I]$_{63}$ line flux by fitting the combined, continuum-subtracted spectra with a Gaussian profile.

We processed the data using different channel binning, continuum subtractions, and weighting of individual data sets; we find the line detection to be robust. To account for the atmospheric features, we report the detection with respect to the noise calculated directly from the scatter in the data (gray shading in Figure 1, rather than the system temperature from GILDAS.

Converting the antenna temperature into flux density using the antenna conversion factor of 70 Jy K^{-1}, we obtain a line flux of $I_{\rm [OI]63} = 22 \pm 5$ Jy km s^{-1}, with FWHM = 130 ± 40 km s^{-1}. This corresponds to a sky-plane [O I]$_{63}$ luminosity of $L_{\rm [OI]} = (5.4 \pm 1.2) \times 10^{10}\ L_\odot$. Adjusting for the FIR-based magnification of $\mu_{\rm FIR} = 9.3 \pm 1.0$ (Zavala et al. 2018b), this translates to a source-plane luminosity of $L_{\rm [OI]} = (5.8 \pm 1.3) \times 10^9\ L_\odot$.

[5] http://www.iram.fr/IRAMFR/GILDAS/

[6] Although APEX observations cannot distinguish between the emission from the source and the $z = 0.776$ lensing galaxy, our detection does not correspond to any potential emission lines for the foreground lens.

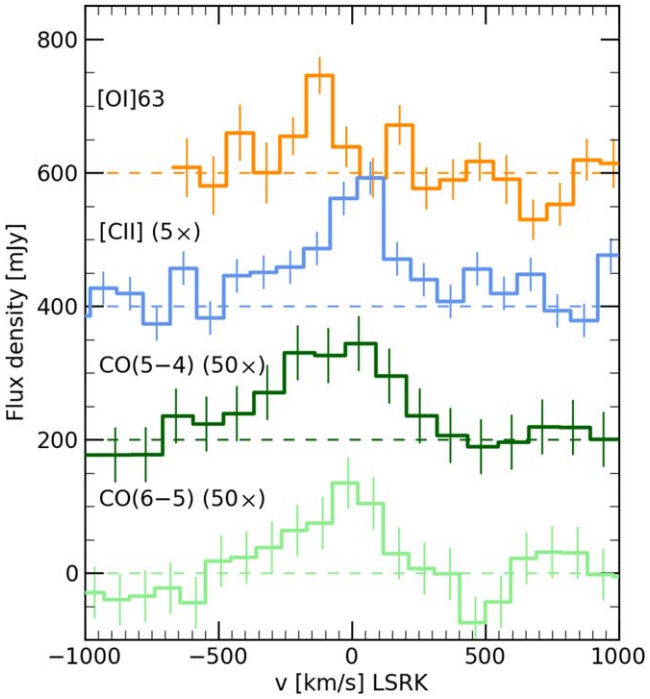

Figure 2. Comparison of the [O I]$_{63}$ spectrum to the [C II] and CO(6–5) and (5–4) line profiles from Zavala et al. (2018b). The [O I]$_{63}$] line is noticeably narrower than the [C II] and CO emission, and tentatively offset from the [C II] line peak. All spectra have been resampled to 100 km s^{-1} bins and are offset by 200 mJy for clarity. The velocities are given in the LSRK frame, using the optical definition.

We do not measure the rest-frame 63 μm continuum flux-density, due to the limited total-power stability of the SEPIA 660 receiver.

3.2. Comparison to [CII] and CO Lines

We now compare our [O I]$_{63}$ line to the [C II], CO(6–5), and (5–4) spectra from Zavala et al. (2018b). As all the line observations are unresolved, we assume the same magnification factor as for the FIR continuum. The two-image configuration of G09.83808 limits the effect of differential lensing, as the magnification does not vary dramatically across the source. However, high-resolution studies of $z \geqslant 2$ DSFGs have shown that the [C II] emission can be substantially more extended than the FIR continuum (Gullberg et al. 2018; Lamarche et al. 2018; Litke et al. 2019; Rybak et al. 2019a, 2019b), and thus only a fraction of the [C II] emission might be associated with the [O I]$_{63}$ and FIR emission.

Compared to the [C II] luminosity from Zavala et al. (2018b), the [O I]$_{63}$ line is $\sim$4 times brighter, and 100 times brighter than the CO(6–5)/(5–4) and H_2O lines. Therefore, the [O I]$_{63}$ dominates the gas cooling budget, in agreement with expectations for the dense star-forming ISM in DSFGs (Kaufman et al. 1999, 2006; Narayanan & Krumholz 2017).

Figure 2 compares the [O I]$_{63}$ line to the [C II] and CO(6–5)/(5–4) lines from Zavala et al. (2018b). The [O I]$_{63}$ lines are noticeably narrower than the [C II] and CO emission (FWHM = 340–500 kms^{-1}). The center of the [O I]$_{63}$ line is consistent with the CO(5–4) and CO(6–5) lines, but offset by $\sim$100 km s^{-1} with respect to the [C II] line (Figure 2). Due to the limited signal-to-noise ratio of the data at hand, the variation of the [O I]$_{63}$/[C II] ratio with velocity remains tentative ($\leqslant 3\sigma$ significance). We consider two potential explanations for this discrepancy. First, the [O I]$_{63}$ emission traces only high-density gas in the central starburst, whereas [C II] traces the bulk of the gas reservoir, thanks to its much lower critical density ($\sim$100 cm^{-3}); the varying [O I]$_{63}$/[C II] and [O I]$_{63}$/CO ratios would then suggest a density gradient across the source. Alternatively, the [O I]$_{63}$ line might be absorbed in the red channels as seen in some $z \sim 0$ ULIRGs (see Rosenberg et al. 2015; Díaz-Santos et al. 2017; Herrera-Camus et al. 2018b). A potential [O I]$_{63}$ self-absorption could be confirmed by comparison with the (much weaker) optically thin [O I] 145 μm emission. High-resolution imaging with ALMA and NOEMA will be crucial for disentangling the relative spatial distribution of the [O I], [C II], CO, and FIR emission.

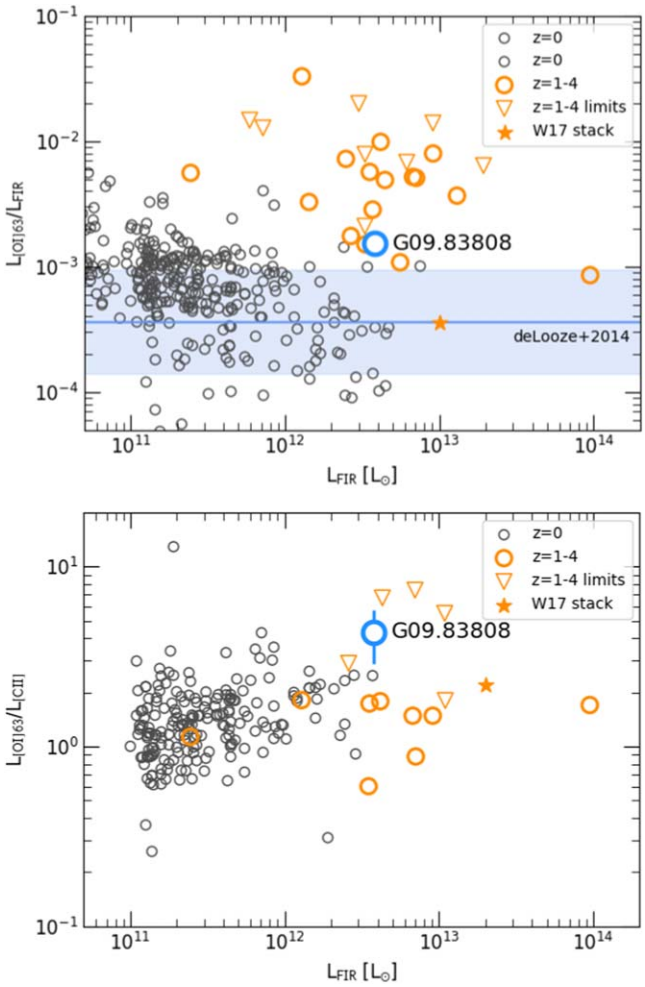

Figure 3. [O I]/FIR (upper) and [O I]/[C II] (lower) luminosity ratios in G09 83808, compared to other high-redshift detections and upper limits and $z \sim 0$ galaxies (GOALS sample from Díaz-Santos et al. 2017 and sources from the Graciá-Carpio et al. 2011 and Coppin et al. 2012 compilation), and the [O I]$_{63}$–FIR correlation from De Looze et al. (2014). The line luminosities are given in units of $L_\odot$. FIR luminosities from the literature have been converted to the 8–1000 μm range. For strongly lensed sources, the luminosities are given as the source plane (de-lensed).

3.3. [OI]/FIR and [OI]/[CII] Ratios

Figure 3 compares the [O I]$_{63}$/FIR and [O I]$_{63}$/[C II] luminosity ratios to literature values for $z \sim 0$ galaxies and $z \geqslant 1$ detections and upper limits. In terms of [O I]$_{63}$/FIR, G09.83808 is in agreement with $z \sim 0$ star-forming galaxies

and ULIRGs (Brauher et al. 2008; Díaz-Santos et al. 2017); contrary to some $z \sim 0$ ULIRGs (Graciá-Carpio et al. 2011; Herrera-Camus et al. 2018b), the [O I]$_{63}$ emission in G09.83808 does not show any [O I]$_{63}$/FIR "deficit." Compared to the *Herschel* [O I]$_{63}$ detections, G09.8308 shows a somewhat lower [O I]$_{63}$/FIR ratio. Rather than indicating that G09.83808 is a special case, this is likely due to a luminosity bias of *Herschel* detections toward [O I]$_{63}$-luminous sources. For example, all the previous $z \geqslant 1$ [O I]$_{63}$ detections—apart from the Wardlow et al. (2017) stack—show a higher [O I]$_{63}$/FIR ratio than the star-forming galaxies from the GOALS sample (Figure 3). Comparing the observed [O I]$_{63}$ luminosity with the FIR-based SFR estimate, G09.83808 falls slightly above the general De Looze et al. (2014) SFR–$L_{[OI]63}$ relation, assuming a Salpeter IMF.

The high [O I]$_{63}$ luminosity also provides an explanation for the observed [C II] cooling deficit. While the [C II] line is typically the main coolant of the neutral ISM with [C II]/FIR ratio of ∼0.5% (comparable to the typical photoelectric heating efficiency), in G09.83808, the observed [C II]/FIR ratio is ∼0.04%. While the low [C II]/FIR ratio has been proposed to be a result of lowered photoelectric heating efficiency due to positive grain charging, this does not seem to be the case in G09.83808: the [O I]$_{63}$ line accounts for ∼0.16% of the total FIR luminosity, and together with the observed [C II], CO, and H_2O lines (i.e., notwithstanding any contribution from other cooling lines), this accounts for ⩾0.2% of the FIR luminosity, in agreement with standard photoelectric heating models (e.g., Bakes & Tielens 1994). Indeed, G09.83808 has the highest [O I]/[C II] ratio among the $z > 1$ detections to date (Figure 3), although consistent with the Wardlow et al. (2017) stack of $z = 1$–4 DSFGs within 2σ. Note that due to the small number of $z > 1$ [O I]$_{63}$ detections, the seven unusually [C II]-bright sources from the Brisbin et al. (2015) sample ($L_{[CII]}/L_{FIR} = (0.4–2.0) \times 10^{-2}$) bias the high-redshift statistics. As the [O I]$_{63}$/[C II] ratio increases with the molecular cloud (surface) density (Narayanan & Krumholz 2017), this suggests a very dense ISM in G09.83808.

3.4. Photodissociation Region (PDR) Modeling

To derive the FUV field strength and density of the neutral ISM from the observed [O I], [C II], and FIR luminosities, we use the PDRToolbox photon-dominated region models (Kaufman et al. 2006; Pound & Wolfire 2008). We adopt the following corrections to the default semi-infinite slab models: (1) as the molecular clouds in DSFGs are likely illuminated both from the front and back, we adjust the PDRToolbox predictions for the optical thickness of individuals tracers: while [C II] and FIR continuum are optically thin and the emission from both the front and back sides of the cloud will be detected, the optically thick [O I]$_{63}$ (and CO) emission will be observed only from the front (see Kaufman et al. 2006; Brisbin et al. 2015; Díaz-Santos et al. 2017; Rybak et al. 2019a; (2) as the [C II] emission can arise from both neutral and ionized gas, we conservatively adjust the [C II] luminosity for 20% ionized gas contribution (see Herrera-Camus et al. 2018b). We adopt the solar-metallicity PDRToolbox model, as FIR indicators point to high ($Z \geqslant 1\,Z_\odot$) metallicity in DSFGs (Wardlow et al. 2017), and as our chosen tracers (FIR, [O I], [C II]) are only weakly dependent on Z (Kaufman et al. 1999).

Figure 4 shows the G-n space traced by the observed [O I]$_{63}$/[C II] and [C II]/FIR ratios, in units of $L_\odot$. In terms of an idealized cloud, the [C II]/FIR is set by G, which determines the depth of the C^+ layer, while the [O I]$_{63}$/[C II] is determined by the gas density.

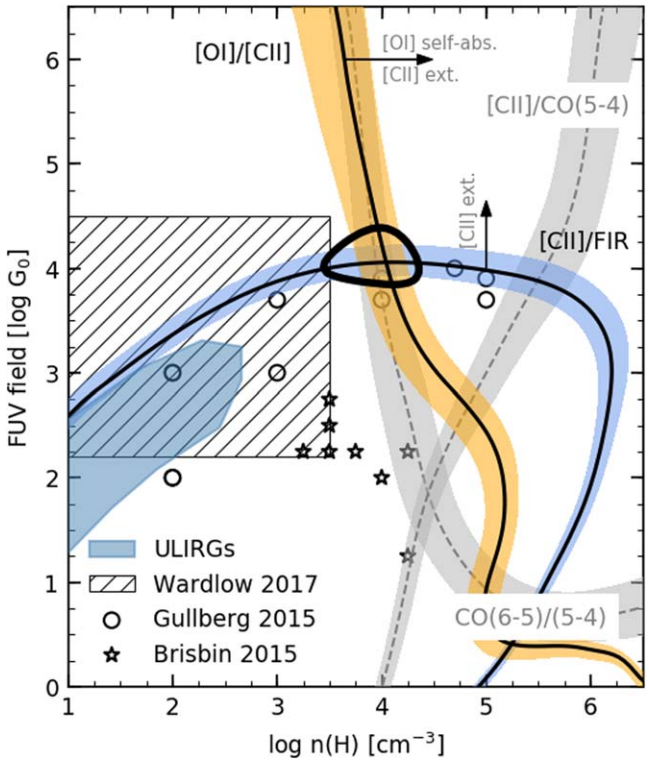

Figure 4. FUV field G and density (n) in G09.83808 inferred using the PDRToolbox models (Kaufman et al. 2006; Pound & Wolfire 2008), compared to other unresolved studies of DSFGs at $z = 1$–5 (Brisbin et al. 2015; Gullberg et al. 2015; Wardlow et al. 2017), and $z \sim 0$ ULIRGs from Díaz-Santos et al. (2017). The thick black line indicates the 1σ confidence region. The [C II]/CO(5–4) and CO(6–5)/CO(5–4) line ratios are not used in the PDR modeling. The arrows indicate the direction (not magnitude) of the contours shifting if the [C II] emission is significantly more extended than FIR continuum, or if [O I]$_{63}$ is self-absorbed.

We obtain a best-fitting model of $G = 10^{4.0\pm0.3}\,G_0$, $n = 10^{4.0\pm0.5}\,\mathrm{cm}^{-3}$. Assuming an optically thin [O I]$_{63}$ emission shifts the best-fitting G value by ∼0.1 dex, while n decreases by ∼0.5 dex. Changing the ionized-phase contribution to the [C II] emission moves the G, n values by ∼0.1 dex. The derived FUV field and density are comparable to the ISM conditions in $z = 1$–4 DSFGs inferred from the fine-structure lines (Wardlow et al. 2017) and [C II] and CO emission (Gullberg et al. 2015), while they are ∼1 dex higher than in $z \sim 0$ ULIRGs (Díaz-Santos et al. 2017; and $z \geqslant 1$ source from Brisbin et al. 2015, inferred from [C II] and [O I]$_{63}$). The difference with the Brisbin et al. (2015) sample is mainly due to their high [C II]/FIR ratios, which determine the G estimates.

Although the CO(5–4) and CO(6–5) lines were excluded from the PDR modeling, the CO(6–5)/(5–4) ratio is consistent with our solution. This is not surprising, as the ratio of the two lines depends mainly on the gas density and is basically unaffected by the CMB (da Cunha et al. 2013). On the other hand, the [C II]/CO(5–4) ratio is offset to much higher densities ($n \simeq 10^5\,\mathrm{cm}^{-3}$ for $G = 10^4\,G_0$). Given the strong dependence of the predicted mid-/high-J CO luminosity to the elevated CMB temperature (da Cunha et al. 2013), which would shift the [C II]/CO(5–4) isocontour to lower densities, we do not consider this discrepancy to be significant.

If the [C II] emission is significantly more extended as the FIR continuum, the total [C II] luminosity associated with the FIR-traced star-forming region will decrease. These would push the PDR model toward higher G and n. Similarly, if a significant fraction of the $[\mathrm{O\,I}]_{63}$ line is self-absorbed, the intrinsic $[\mathrm{O\,I}]_{63}$ luminosity will increase, moving the best-fitting model to higher densities.

3.5. Detecting the [OI] 63 μm Emission from z ≳6 DSFGs with ALMA

What are the prospects of detecting the $[\mathrm{O\,I}]_{63}$ line from $z \geqslant 6$ non-lensed DSFGs with ALMA Band 9 observations?

Assuming that the intrinsic (i.e., de-lensed) properties of G09.83808 are representative of the $z \geqslant 6$ DSFG population, i.e., with $[\mathrm{O\,I}]_{63}$ source-plane luminosity of $5.8 \times 10^9\,L_\odot$ over $\sim$100 km s^{-1} line width, the $[\mathrm{O\,I}]_{63}$ emission will be detectable at $\geqslant 5\sigma$ level in less than 15 minutes on-source time. At $z \geqslant 6.8$, the $[\mathrm{O\,I}]_{63}$ shifts outside Band 9, and is only redshifted into Band 8 at $z \geqslant 8.5$, when the required on-source time increases into hours. In contrast to G09.83808-like sources, detecting the $[\mathrm{O\,I}]_{63}$ emission from normal star-forming galaxies such as the population from the Olsen et al. (2017) simulations (SFR = 2–20 $M_\odot$ yr^{-1}, $L_{[\mathrm{OI}]63} = (0.3\text{–}2.0) \times 10^8\,L_\odot$) remains prohibitively expensive.

The modest expense of ALMA time required to detect the $[\mathrm{O\,I}]_{63}$ emission from G09.83808-like DSFGs will allow an efficient follow-up of $z \gtrsim 6$ DSFGs, which will be delivered by the ongoing and planned millimeter-wave surveys (e.g., Casey et al. 2018; Zavala et al. 2018a; Magnelli et al. 2019). The combination of the $[\mathrm{O\,I}]_{63}$ and [C II] emission lines with the FIR continuum will then provide robust measurements of the FUV field and gas density in their star-forming regions.

4. Conclusions

We have obtained the first ground-based detection of the [O I] 63 μm emission from a $z \geqslant 6$ galaxy, using APEX SEPIA 660 spectroscopy, with only 2:15 hr on-source time. This represents the first unambiguous $[\mathrm{O\,I}]_{63}$ detection beyond redshift 3. In combination with the FIR continuum and [C II] and CO(6–5)/(5–4) observations from Zavala et al. (2018b), this detection allows us to constrain the physical conditions of the star-forming ISM. Our main findings are:

1. The $[\mathrm{O\,I}]_{63}$ line dominates the neutral gas cooling budget, with a [O I]/[C II] ratio of $\sim$4. The shift of the main cooling channel from the [C II] to the $[\mathrm{O\,I}]_{63}$ line is in agreement with radiative transfer models of star-forming galaxies (e.g., Kaufman et al. 1999, 2006; Narayanan & Krumholz 2017; Olsen et al. 2017). The cooling via the $[\mathrm{O\,I}]_{63}$ line compensates for the pronounced [C II] deficit in G09.83808; the total $[\mathrm{O\,I}]_{63}$+[C II]+CO cooling corresponds to $\geqslant$0.2% of the FIR luminosity
2. The $[\mathrm{O\,I}]_{63}$ line profile is significantly narrower than the [C II] and CO(6–5)/(5–4) lines, and blueshifted by $\sim$100 km s^{-1} with respect to the [C II] emission. If real, this can be either due to the varying conditions across the source (density in particular), or a self-absorption of the $[\mathrm{O\,I}]_{63}$ line in the red channels (implying an even higher intrinsic $[\mathrm{O\,I}]_{63}$ luminosity). Future [C II] and $[\mathrm{O\,I}]_{63}/[\mathrm{O\,I}]_{145}$ observations are necessary to distinguish between the two scenarios.
3. Using the photon-dissociation region models of Kaufman et al. (2006) and Pound & Wolfire (2008), we derive a source-averaged FUV field strength $G = 10^4\,G_0$ and density $n = 10^{4.0}$ cm^{-3}. These are comparable to source-averaged values for $z = 1$–4 DSFG samples, and are $\geqslant$1 dex higher than source-averaged values in $z \sim 0$ ULIRGs.
4. If G09.83808 represents a typical $z \sim 6$ DSFG, a 5σ detection of the $[\mathrm{O\,I}]_{63}$ emission from a $z = 6$ non-lensed DSFGs will be possible in $\sim$15 minutes of ALMA Band 9 observations, complementing the currently exploited [C II] and [O III] emission.

These results highlight the power of the [O I] 63 μm line as a tracer of neutral ISM in DSFGs at the highest redshift. Thanks to its brightness, ground-based studies of the [O I] 63 μm line will open a new window into the physics of star-forming neutral ISM in the first billion years of cosmic history.

The authors thank Kalle Torstensson and Carlos de Breuck for carrying out observations used in this work and their comments on early version of this manuscript. This publication is based on data acquired with the Atacama Pathfinder Experiment (APEX) and the APEX SEPIA receiver, developed by NOVA, the Netherlands Research School for Astronomy. APEX is a collaboration between the Max-Planck-Institut für Radioastronomie, the European Southern Observatory, and the Onsala Space Observatory. M.R. and J.H. acknowledge support of the VIDI research programme with project number 639.042.611, which is (partly) financed by the Netherlands Organisation for Scientific Research (NWO). C.M.C. thanks the National Science Foundation for support through grants AST-1714528 and AST-1814034, and additionally C.M.C. and J.A.Z. thank the University of Texas at Austin College of Natural Sciences for support. In addition, C.M.C. acknowledges support from the Research Corporation for Science Advancement from a 2019 Cottrell Scholar Award sponsored by IF/THEN, an initiative of Lyda Hill Philanthropies.

Facility: APEX.

ORCID iDs

Matus Rybak https://orcid.org/0000-0002-1383-0746
J. A. Zavala https://orcid.org/0000-0002-7051-1100
J. A. Hodge https://orcid.org/0000-0001-6586-8845
C. M. Casey https://orcid.org/0000-0002-0930-6466
P. van der Werf https://orcid.org/0000-0001-5434-5942

References

Bakes, E. L. O., & Tielens, A. G. G. M. 1994, ApJ, 427, 822
Belitsky, V., Lapkin, I., Fredrixon, M., et al. 2018, A&A, 612, A23
Brauher, J. R., Dale, D. A., & Helou, G. 2008, ApJS, 178, 280
Brisbin, D., Ferkinhoff, C., Nikola, T., et al. 2015, ApJ, 799, 13
Carniani, S., Maiolino, R., Pallottini, A., et al. 2017, A&A, 605, A42
Casey, C. M., Narayanan, D., & Cooray, A. 2014, PhR, 541, 45
Casey, C. M., Zavala, J. A., Spilker, J., et al. 2018, ApJ, 862, 77
Coppin, K. E. K., Danielson, A. L. R., Geach, J. E., et al. 2012, MNRAS, 427, 520
da Cunha, E., Groves, B., Walter, F., et al. 2013, ApJ, 766, 13
De Looze, I., Cormier, D., Lebouteiller, V., et al. 2014, A&A, 568, A62
Decarli, R., Walter, F., Venemans, B. P., et al. 2017, Natur, 545, 457
Díaz-Santos, T., Armus, L., Charmandaris, V., et al. 2017, ApJ, 846, 32
Graciá-Carpio, J., Sturm, E., Hailey-Dunsheath, S., et al. 2011, ApJL, 728, L7
Gullberg, B., De Breuck, C., Vieira, J. D., et al. 2015, MNRAS, 449, 2883
Gullberg, B., Swinbank, A. M., Smail, I., et al. 2018, ApJ, 859, 12
Harikane, Y., Ouchi, M., Inoue, A. K., et al. 2019, arXiv:1910.10927

Hashimoto, T., Inoue, A. K., Mawatari, K., et al. 2019, PASJ, 71, doi:10.1093/pasj/psz049
Herrera-Camus, R., Sturm, E., Graciá-Carpio, J., et al. 2018a, ApJ, 861, 94
Herrera-Camus, R., Sturm, E., Graciá-Carpio, J., et al. 2018b, ApJ, 861, 95
Hesper, R., Khudchenko, A., Baryshev, A. M., Barkhof, J., & Mena, F. P. 2017, ITTST, 7, 686
Hesper, R., Khudchenko, A., Lindemulder, M., et al. 2018, ITTST, 8, 1, https://www.nrao.edu/meetings/isstt/papers/2018/2018098103.pdf
Hodge, J. A., Karim, A., Smail, I., et al. 2013, ApJ, 768, 91
Inoue, A. K., Tamura, Y., Matsuo, H., et al. 2016, Sci, 352, 1559
Ivison, R. J., Smail, I., Papadopoulos, P. P., et al. 2010, MNRAS, 404, 198
Katz, H., Galligan, T. P., Kimm, T., et al. 2019, MNRAS, 487, 5902
Kaufman, M. J., Wolfire, M. G., & Hollenbach, D. J. 2006, ApJ, 644, 283
Kaufman, M. J., Wolfire, M. G., Hollenbach, D. J., & Luhman, M. L. 1999, ApJ, 527, 795
Kennicutt, & Robert C., J. 1998, ARA&A, 36, 189
Lamarche, C., Verma, A., Vishwas, A., et al. 2018, ApJ, 867, 140
Litke, K. C., Marrone, D. P., Spilker, J. S., et al. 2019, ApJ, 870, 80
Magnelli, B., Karim, A., Staguhn, J., et al. 2019, ApJ, 877, 45
Narayanan, D., & Krumholz, M. R. 2017, MNRAS, 467, 50
Olsen, K., Greve, T. R., Narayanan, D., et al. 2017, ApJ, 846, 105
Planck Collaboration, Ade, P. A. R., Aghanim, N., et al. 2016, A&A, 594, A13
Popping, G., Narayanan, D., Somerville, R. S., Faisst, A. L., & Krumholz, M. R. 2019, MNRAS, 482, 4906
Pound, M. W., & Wolfire, M. G. 2008, in ASP Conf. Ser. 394, Astronomical Data Analysis Software and Systems XVII, ed. R. W. Argyle, P. S. Bunclark, & J. R. Lewis (San Francisco, CA: ASP), 654
Riechers, D. A., Bradford, C. M., Clements, D. L., et al. 2013, Natur, 496, 329
Rosenberg, M. J. F., van der Werf, P. P., Aalto, S., et al. 2015, ApJ, 801, 72
Rybak, M., Calistro Rivera, G., Hodge, J. A., et al. 2019a, ApJ, 876, 112
Rybak, M., Hodge, J. A., Vegetti, S., et al. 2019b, arXiv:1912.12538
Smit, R., Bouwens, R. J., Carniani, S., et al. 2018, Natur, 553, 178
Stacey, G. J., Hailey-Dunsheath, S., Ferkinhoff, C., et al. 2010, ApJ, 724, 957
Strandet, M. L., Weiss, A., De Breuck, C., et al. 2017, ApJL, 842, L15
Sturm, E., Verma, A., Graciá-Carpio, J., et al. 2010, A&A, 518, L36
Wardlow, J. L., Cooray, A., Osage, W., et al. 2017, ApJ, 837, 12
Wright, E. L. 2006, PASP, 118, 1711
Yang, C., Gavazzi, R., Beelen, A., et al. 2019, A&A, 624, A138
Zavala, J. A., Casey, C. M., da Cunha, E., et al. 2018a, ApJ, 869, 71
Zavala, J. A., Montaña, A., Hughes, D. H., et al. 2018b, NatAs, 2, 56
Zhang, Z.-Y., Ivison, R. J., George, R. D., et al. 2018, MNRAS, 481, 59